Acta Astronautica 181 (2021) 733–740

Contents lists available at ScienceDirect

Acta Astronautica

journal homepage: www.elsevier.com/locate/actaastro

Adaptive control for differential drag-based rendezvous maneuvers with an unknown target

Camilo Riano-Rios [a,*], Riccardo Bevilacqua [a,**], Warren E. Dixon [b]

[a] University of Florida, 939 Sweetwater Dr., Gainesville, FL, USA
[b] University of Florida, 633 Gale Lemerand Dr., Gainesville, FL, USA

ARTICLE INFO

Keywords:
Differential drag
Adaptive
Atmospheric density
Drag coefficient
Rendezvous
Ballistic coefficient

ABSTRACT

This paper presents a differential atmospheric drag-based control algorithm for rendezvous with a non-cooperative target in Low Earth Orbit. The challenge of using a differential input that requires knowledge of physical parameters of the involved spacecraft, is addressed by designing a Lyapunov-based adaptive controller that compensates for the uncertain ballistic coefficient of the target spacecraft as well as the time-varying atmospheric density and velocity of the spacecraft relative to the atmosphere. Numerical simulations using the Schweighart-Sedwick relative dynamics are presented to validate the controller design. Additionally, simulations with more accurate dynamics for each spacecraft along with the NRLMSISE-00 model of atmospheric density are presented to evaluate the performance of the controller under nonlinearities and input saturation.

1. Introduction

The increasing number of spacecraft in Low Earth Orbit (LEO) has been a matter of concern for orbital debris mitigation. A large number of satellites in LEO are CubeSats with very limited propulsion capabilities to accomplish their intended missions. Once these satellites are out of operation or malfunctioned, it is desirable to have them safely removed from orbit and respecting the NASA requirement for LEO satellites to de-orbit within 25 years [1]. This paper focuses on the challenge of performing propellant-less rendezvous with a non-cooperative spacecraft once it has been detected and identified as a potential target.

The acceleration due to differential drag between two satellites in LEO has been identified as a potential resource to perform relative maneuvers. The development of differential drag-based strategies to perform relative maneuvers has been an active focus of research since it was first presented back in 1989 [2] and has acquired even more importance due to the introduction of the CubeSat standard. One of the major challenges of using differential drag to perform formation and rendezvous maneuvers is that its performance is highly dependent on the knowledge of parameters that have important levels of uncertainty, such as the atmospheric density and drag coefficient.

Open-loop analytical algorithms have been developed for relative maneuvers between controllable spacecraft [2–5]. On the other hand, a wide variety of closed loop control algorithms have also been developed for this purpose [6–9]. Implementations of differential drag-based algorithms for formation keeping maneuvers such as those of the ORBCOMM [10] and Planet Labs [11] constellations have demonstrated its effectiveness. However, since the computation of the differential drag acceleration requires knowledge of the area-to-mass ratio of the involved spacecraft, namely their ballistic coefficient, the development of control algorithms to perform differential drag-based rendezvous maneuvers with a spacecraft with uncertain ballistic coefficient is still a matter of study. Thruster-based algorithms for rendezvous with uncooperative spacecraft have been presented in different works such as [12–15], where autonomous relative navigation and guidance strategies have been presented and even demonstrated in orbit [16].

The Drag De-Orbit Device (D3), originally designed at University of Florida ADvanced Autonomous MUltiple Spacecraft (ADAMUS) laboratory for spacecraft controlled re-entry [17–19], has also shown to have potential for spacecraft relative maneuvers [3,9] and passive attitude stabilization [20,21]. Motivated by these efforts and the potential of the differential drag for saving propellant, we present a novel approach to perform differential drag-based rendezvous maneuvers with an unknown target using a D3-equipped 2U CubeSat.

The D3 can be installed in the anti-ram face of the CubeSat and has four repeatedly deployable/retractable drag surfaces offset 90° from

* Corresponding author.
** Corresponding author.
E-mail addresses: crianorios@ufl.edu (C. Riano-Rios), bevilr@ufl.edu (R. Bevilacqua).

https://doi.org/10.1016/j.actaastro.2020.03.011
Received 4 March 2020; Accepted 9 March 2020
Available online 19 March 2020

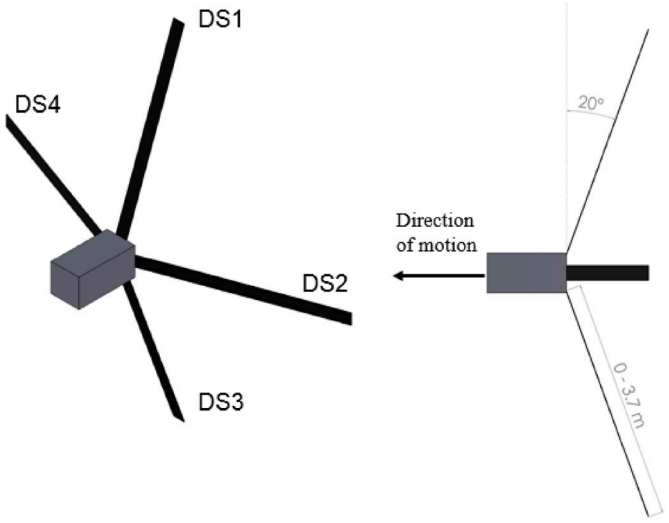

Fig. 1. Drag De-orbit device (D3) schematic.

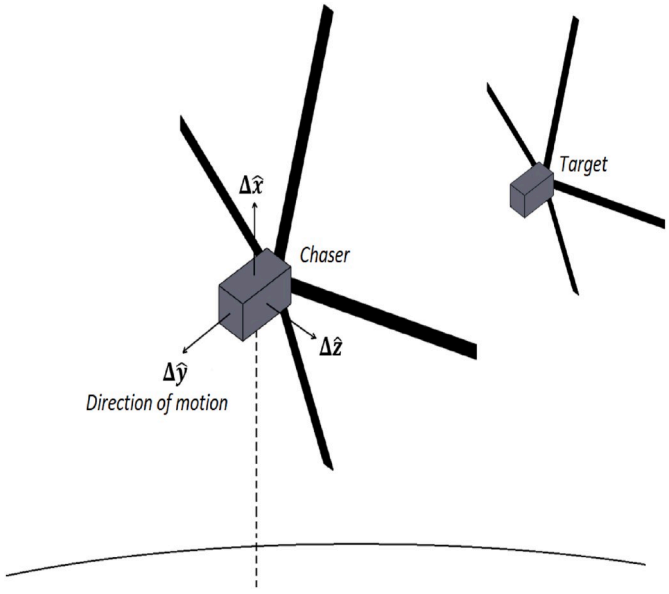

Fig. 2. LVLH coordinate system.

each other and inclined 20°, a simplified schematic of the D3 device is shown in Fig. 1. The proposed control algorithm uses a Lyapunov-based adaptive update law to compensate for the uncertain time-varying atmospheric density, velocity of the spacecraft relative to the atmosphere and ballistic coefficient of the target spacecraft, to drive the controllable (chaser) spacecraft to the position of the target. The maneuvers are limited to be between spacecraft in circular LEO orbits, in the same orbit plane and for small inter-spacecraft distances compared with the semi-major axis of the chaser spacecraft. Additionally, it is assumed throughout the paper that the relative states are measurable and the ballistic coefficient of the target is somewhere between maximum and minimum limits for the ballistic coefficient of the chaser spacecraft, i.e. a rough estimate of this parameter is available a priori to determine the feasibility of the maneuver.

The main contributions of this work are:

- An adaptive control policy that ensures asymptotic stability of the in-plane relative states despite uncertainty in the physical parameters of the target spacecraft.
- The adaptive update laws additionally consider the unknown time-varying atmospheric density and magnitude of spacecraft-atmosphere relative velocity for both spacecraft.
- A strategy that uses a propellant-less differential control input with respect to an unknown spacecraft.
- Controller design validation using numerical simulations with higher fidelity dynamics and additional perturbations for each spacecraft.
- A control law that is completely implementable on-board with very low computational cost since it does not use iterative algorithms nor complex atmospheric models.

The paper is organized as follows: Section 2 presents the dynamic models used for control design and numerical simulations, Section 3 shows the control design, Section 4 presents the corresponding stability analysis and Sections 5 and 6 show the numerical simulations and conclusions, respectively.

2. Dynamics modeling

2.1. Spacecraft relative dynamics

The acceleration experienced by a spacecraft in LEO under the gravitational influence of the Earth as well as the J_2 perturbation and atmospheric drag can be expressed in the Earth-Centered Inertial (ECI) coordinate system as follows

$$\ddot{x} = -\frac{GM_\oplus}{r^3}x + \frac{3}{2}\left(\frac{J_2 GM_\oplus R_\oplus^2}{r^4}\right)\left(\frac{x}{r}\left(\frac{5z^2}{r^2}-1\right)\right) + \ddot{r}_{drag,x} \tag{1}$$

$$\ddot{y} = -\frac{GM_\oplus}{r^3}y + \frac{3}{2}\left(\frac{J_2 GM_\oplus R_\oplus^2}{r^4}\right)\left(\frac{y}{r}\left(\frac{5z^2}{r^2}-1\right)\right) + \ddot{r}_{drag,y} \tag{2}$$

$$\ddot{z} = -\frac{GM_\oplus}{r^3}z + \frac{3}{2}\left(\frac{J_2 GM_\oplus R_\oplus^2}{r^4}\right)\left(\frac{z}{r}\left(\frac{5z^2}{r^2}-3\right)\right) + \ddot{r}_{drag,z} \tag{3}$$

where $\ddot{\boldsymbol{r}}_{drag} = [\ddot{r}_{drag,x}, \ddot{r}_{drag,y}, \ddot{r}_{drag,z}]^T$ is the acceleration due to atmospheric drag expressed in the ECI coordinate system, G is the universal gravitational constant, $\boldsymbol{r} = [x, y, z]^T$ is the ECI position of the spacecraft, J_2 is the coefficient that represents the second order harmonic of gravitational potential field of the Earth, $M_\oplus$ and $R_\oplus$ are the mass and radius of the Earth, respectively.

Assumption 1. The chaser spacecraft is ram-aligned, the inter-spacecraft distance is small compared with its orbit radius and the two involved spacecraft are in the same circular LEO orbit plane.

Under Assumption 1, the relative motion between the two spacecraft can be expressed in the Local-Vertical/Local-Horizontal LVLH coordinate system (Fig. 2) using the linear Schweighart-Sedwick (SS) [22] dynamic model that includes the influence of the J_2 perturbation as

$$\Delta\ddot{x} = 2(\Omega c)\Delta\dot{y} + \left(5c^2 - 2\right)\Omega^2\Delta x + u_x \tag{4}$$

$$\Delta\ddot{y} = -2(\Omega c)\Delta\dot{x} + u_y \tag{5}$$

$$\Delta\ddot{z} = -q^2\Delta z + 2lq\cos(qt + \phi) + u_z \tag{6}$$

where Ω is the constant angular velocity of the orbit of the chaser, $\boldsymbol{\Delta r} = [\Delta x, \Delta y, \Delta z]^T$ is the LVLH position of the target, $\boldsymbol{u} = [u_x, u_y, u_z]^T$ is the control input (differential drag), and c is defined as

$$c = \sqrt{1 + \frac{3J_2 R_\oplus^2}{8r_{ref}^2}\left(1 + 3\cos\left(2i_{ref}\right)\right)} \tag{7}$$

where r_{ref} and i_{ref} are the radius and inclination of the orbit of the chaser.

The parameters ϕ, l and q in the out-of-plane equation of motion (6) are defined in Ref. [22].

Assumption 2. The chaser spacecraft is capable of measuring the in-

Table 1
Initial conditions for the chaser spacecraft.

a_c [km]	e_c	i_c [deg]	Ω_c [deg]	ω_c [deg]	ν_c [deg]
6.7131×10^3	0	51.94	206.36	101.07	108.08

Table 2
Controller parameters.

Q	R	Γ_1	Γ_2
$diag(180, 1, 1.8, 1)$	1.8×10^{16}	$1 \times 10^{-21} \times I_{3\times3}$	$1.5 \times 10^{-21} \times I_{3\times3}$

Table 3
Spacecraft physical parameters.

S_t [m^2]	m_t [kg]	$S_{c,max}$ [m^2]	$S_{c,min}$ [m^2]	m_c [kg]
0.2	1.5	0.5	0.01	3

Table 4
Parameter values for density model.

$D_{1,i}$ [kg/m^3]	$D_{2,i}$ [kg/m^3]	$D_{3,i}$ [kg/m^3]
3.3319×10^{-12}	-7.1895×10^{-13}	1.3008×10^{-13}

plane relative states of the target using sensors and estimation techniques, e.g. similar to those in Ref. [12,16].

The LVLH coordinate system can then be defined to be attached to the chaser spacecraft with origin at its center of mass and defined as follows: The $\Delta\hat{x}$ axis points from the center of the Earth towards the origin of the system, the $\Delta\hat{z}$ axis is aligned with the orbit angular momentum vector and the $\Delta\hat{y}$ completes a right-hand Cartesian coordinate system.

2.2. Differential drag

The chaser D3-equipped spacecraft is capable of changing its experienced drag acceleration by repeatedly extending/retracting the drag surfaces (Fig. 1). The acceleration due to atmospheric drag acting on a spacecraft can be expressed as

$$\ddot{\boldsymbol{r}}_{drag} = -\rho(t) C_b V_r^2 \hat{\boldsymbol{V}}_r \tag{8}$$

where $\rho(t)$ represents the time-varying atmospheric density and C_b is the ballistic coefficient of the spacecraft defined as

$$C_b = \frac{SC_D}{2m}, \tag{9}$$

the parameter C_D is the drag coefficient, S and m are the total cross-sectional area and mass of the spacecraft, respectively. Then, the ballistic coefficient of the chaser spacecraft can be changed by modulating the cross-sectional area S, i.e. extending/retracting the drag surfaces.

The vector $\boldsymbol{V}_r$ represents the velocity of the spacecraft relative to the atmosphere which is assumed to rotate with the Earth and is defined as follows

$$\boldsymbol{V}_r = \dot{\boldsymbol{r}} - \boldsymbol{\omega}_{\oplus} \times \boldsymbol{r} \tag{10}$$

where $\boldsymbol{\omega}_{\oplus}$ is the angular velocity of the Earth.

The auxiliary control input $\boldsymbol{u}$, namely the differential drag, is then defined as

$$\boldsymbol{u} = \Delta\ddot{\boldsymbol{r}}_{drag} = \ddot{\boldsymbol{r}}_{drag,t} - \ddot{\boldsymbol{r}}_{drag,c} \tag{11}$$

where the subscripts c and t make reference to the chaser and the target spacecraft, respectively.

The atmospheric density $\rho(t)$ is the greatest source of uncertainty in the computation of the experienced drag acceleration due to its dependence on several environmental variables such as geomagnetic and solar activity, as well as to the orbital motion. There exist several models to estimate the local atmospheric density with different levels of uncertainty, some are function of the altitude and theoretical models of the upper atmosphere such as the 1976 U.S Standard [23] and the Harris-Priester [24] models, whereas more complex empirical models, such as the NRLMSISE-00 [25] are function of the position of the spacecraft, date, time, solar and geomagnetic indices. However, even the more complex atmospheric models require considerable computational effort and still provide limited accuracy [26]. The latter motivates the design of adaptive controllers that do not require information about such uncertain parameters to guarantee the maneuver success.

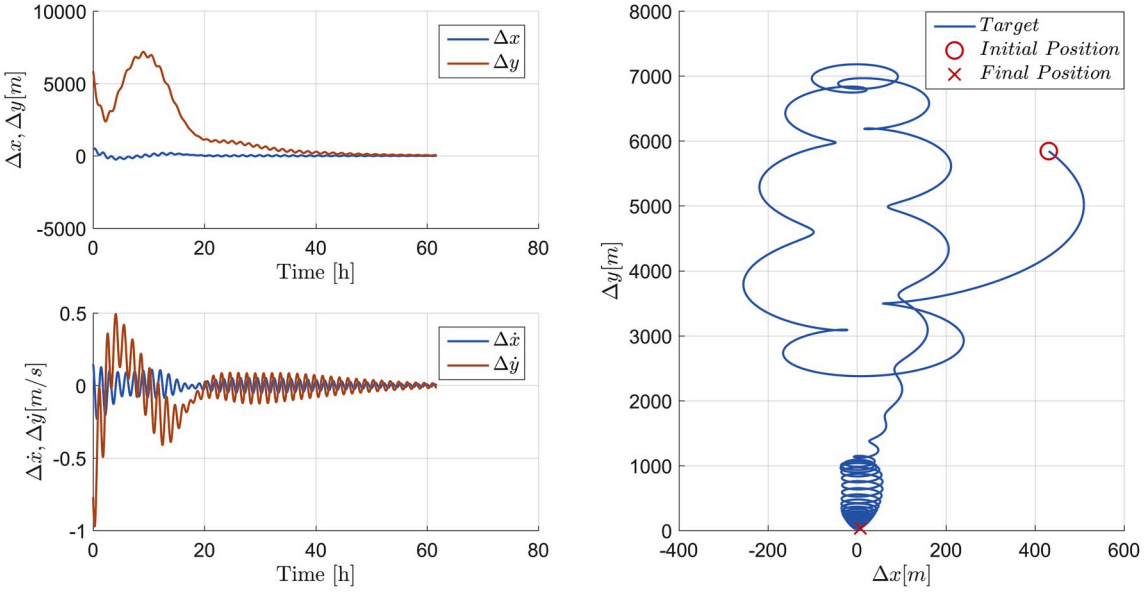

Fig. 3. Resulting relative states using the SS dynamics.

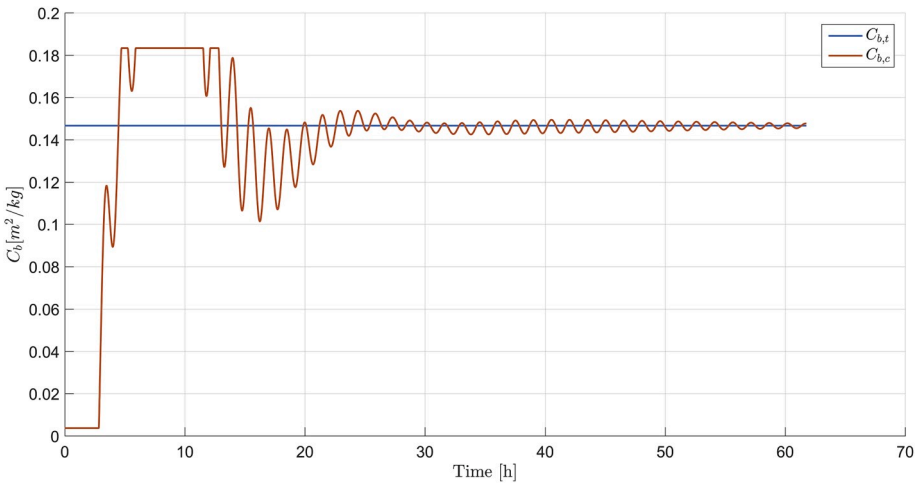

Fig. 4. Control command using the SS dynamics.

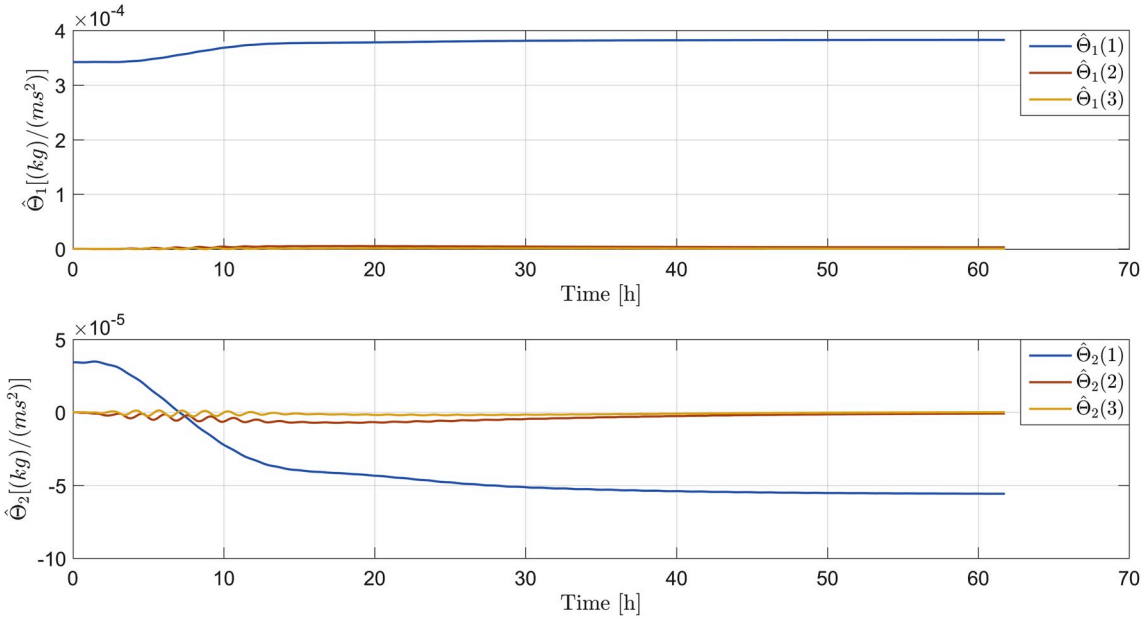

Fig. 5. Estimated parameters using the SS dynamics.

3. Control design

3.1. Control objective

The control objective is to complete a rendezvous maneuver between a controllable D3-equipped spacecraft (chaser) and a non-cooperative spacecraft (target), using the differential drag as the only control input without relying on precise information about the physical parameters of the unknown target ($C_{b,t}$). Additionally, the auxiliary control input $\boldsymbol{u}$ includes uncertainty in the time-varying atmospheric density $\rho(t)$ and the magnitude of the spacecraft-atmosphere relative velocity V_r.

Assumption 3. The ballistic coefficient of the chaser $C_{b,c}$ is known provided that its physical parameters are known, the time-varying local atmospheric density $\rho(t)$ and the (constant) magnitude of the velocity relative to the atmosphere V_r are uncertain for both spacecraft.

Assumption 4. The velocity of the spacecraft relative to the atmosphere $\boldsymbol{V}_r$ is opposite to the LVLH's $\boldsymbol{\Delta\hat{y}}$ direction.

Considering Assumptions 3 and 4, the differential drag can be written as

$$\boldsymbol{u} = \left(\rho_c(t)V_{r,c}^2\overline{u}(t) - \rho_t(t)V_{r,t}^2C_{b,t}\right)\boldsymbol{\Delta\hat{y}} \tag{12}$$

where $\overline{u}(t) = C_{b,c}$ represents the only parameter that can be modified in the control input. Therefore, the only nonzero component of $\boldsymbol{u}$ in equations (4)–(6) is $u_y = \rho_c(t)V_{r,c}^2\overline{u}(t) - \rho_t(t)V_{r,t}^2C_{b,t}$. In Ref. [27], the differential drag between two spacecraft with constant ballistic coefficient was modeled as a time-varying function with its two principal Fourier components at 0 and Ω. Therefore, the behavior over time of the differential drag was dominated by the variation of the atmospheric density. This motivates us to model the parameter $\rho_i(t)$ as

$$\rho_i(t) = D_{1,i} + D_{2,i}\sin(\Omega t) + D_{3,i}\cos(\Omega t)\,, \qquad i = c,t \tag{13}$$

where $D_{1,i}, D_{2,i}, D_{3,i} \in \mathbb{R}$ are unknown constants.

3.2. Control development

From the SS relative dynamics (equations (4)–(6)) and equation (12), since the Δz dynamics are decoupled, only the in-plane (Δx - Δy) motion

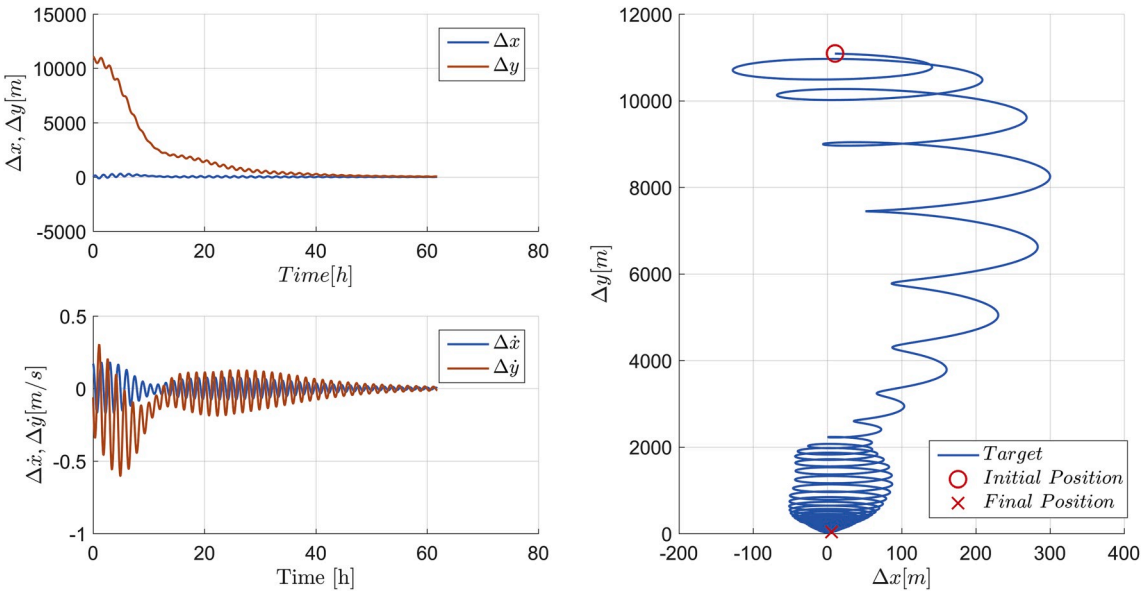

Fig. 6. Resulting relative states using the complete dynamics.

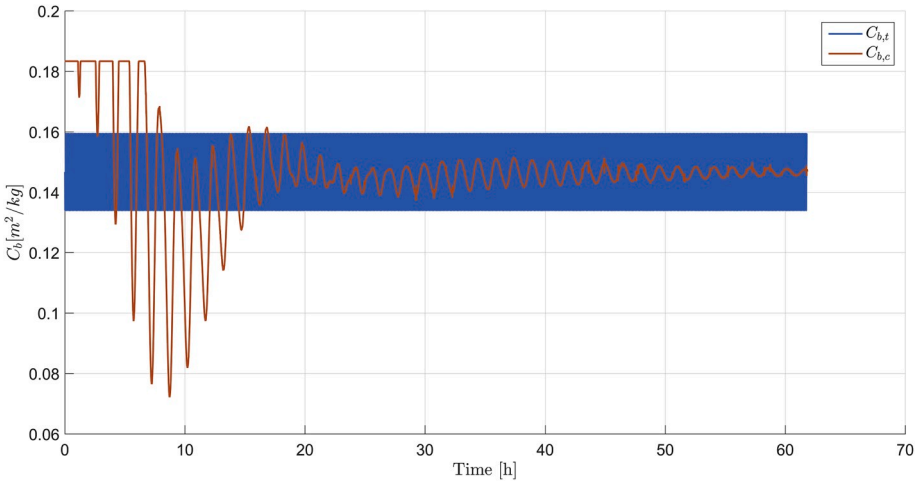

Fig. 7. Control command using the complete dynamics.

can be controlled by means of differential drag. The state space representation of the in-plane relative dynamics is

$$\underbrace{\begin{bmatrix}\Delta\dot{x}\\ \Delta\ddot{x}\\ \Delta\dot{y}\\ \Delta\ddot{y}\end{bmatrix}}_{\dot{X}} = \underbrace{\begin{bmatrix}0 & 1 & 0 & 0\\ b & 0 & 0 & a\\ 0 & 0 & 0 & 1\\ 0 & -a & 0 & 0\end{bmatrix}}_{A}\underbrace{\begin{bmatrix}\Delta x\\ \Delta\dot{x}\\ \Delta y\\ \Delta\dot{y}\end{bmatrix}}_{X} + \underbrace{\begin{bmatrix}0\\ 0\\ 0\\ 1\end{bmatrix}}_{B} u_y \tag{14}$$

where $a = 2\Omega c$ and $b = (5c-2)\Omega^2$ are known positive constants.

Let us define two linear parameterizations of the terms in the auxiliary control input u_y as

$$\boldsymbol{Y}_1\boldsymbol{\Theta}_1 = \rho_c(t)V_{r,c}^2\bar{u}(t) \tag{15}$$

$$\boldsymbol{Y}_2\boldsymbol{\Theta}_2 = -\rho_t(t)V_{r,t}^2C_{b,t} \tag{16}$$

Substituting equations (15) and (16) in the definition of u_y yields

$$u_y = \boldsymbol{Y}_1\boldsymbol{\Theta}_1 + \boldsymbol{Y}_2\boldsymbol{\Theta}_2 \tag{17}$$

In equation (15), $\boldsymbol{Y}_1 \in \mathbb{R}^3$ denotes the first measurable regression matrix

$$\boldsymbol{Y}_1(\bar{u}(t),\Omega) = [\bar{u}(t)\ ,\ u(t)\sin(\Omega t)\ ,\ \bar{u}(t)\cos(\Omega t)] \tag{18}$$

and the first vector of uncertain parameters $\boldsymbol{\Theta}_1 \in \mathbb{R}^3$ is

$$\boldsymbol{\Theta}_1 = \begin{bmatrix}D_{1,c}V_{r,c}^2\\ D_{2,c}V_{r,c}^2\\ D_{3,c}V_{r,c}^2\end{bmatrix} \tag{19}$$

On the other hand, in equation (16), $\boldsymbol{Y}_2 \in \mathbb{R}^3$ denotes the second measurable regression matrix

$$\boldsymbol{Y}_2(\Omega) = [-1\ ,\ -sin(\Omega t)\ ,\ -cos(\Omega t)] \tag{20}$$

and the second vector of uncertain parameters is

$$\boldsymbol{\Theta}_2 = \begin{bmatrix}D_{1,t}V_{r,t}^2C_{b,t}\\ D_{2,t}V_{r,t}^2C_{b,t}\\ D_{3,t}V_{r,t}^2C_{b,t}\end{bmatrix}. \tag{21}$$

Considering their physical meaning, the uncertain parameters in the

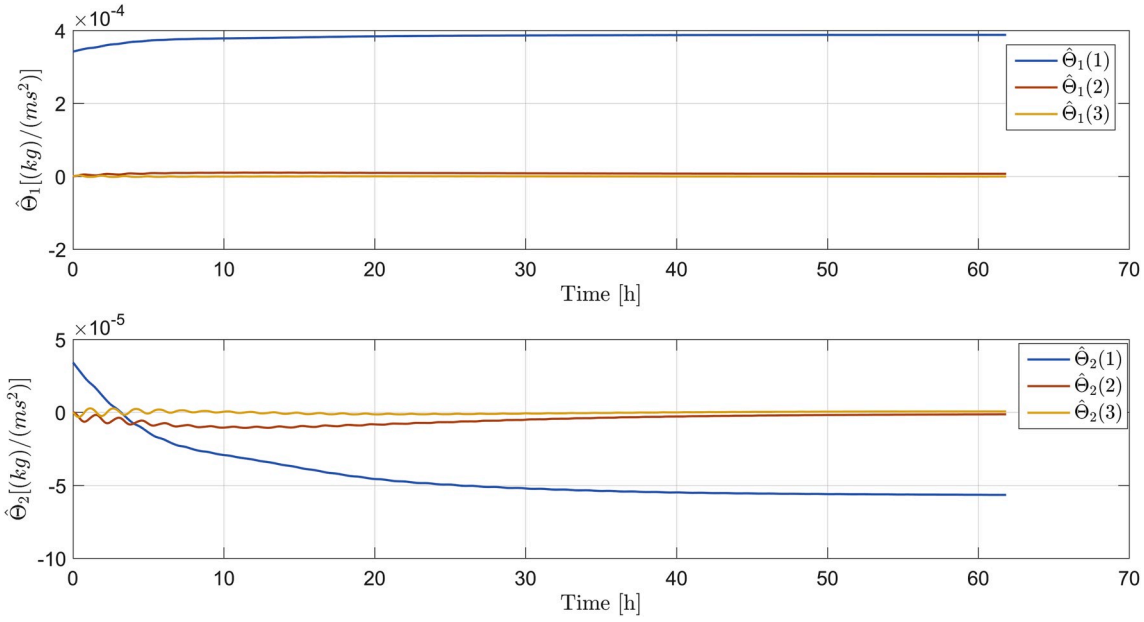

Fig. 8. Estimated parameters using the complete dynamics.

vectors $\boldsymbol{\Theta}_1$ and $\boldsymbol{\Theta}_2$ can upper and lower be bounded as

$$\underline{\Theta}_{1,j} < \Theta_{1,j} < \overline{\Theta}_{1,j} \tag{22}$$

$$\underline{\Theta}_{2,j} < \Theta_{2,j} < \overline{\Theta}_{2,j} \tag{23}$$

where $\Theta_{1,j}$ ($\Theta_{2,j}$) is the j^{th} component of $\boldsymbol{\Theta}_1$ ($\boldsymbol{\Theta}_2$), and $\underline{\Theta}_{1,j}, \underline{\Theta}_{2,j}, \overline{\Theta}_{1,j}, \overline{\Theta}_{2,j} \in \mathbb{R}$ denote the known constant bounds for the corresponding parameter.

The estimates of equations (15) and (16) are

$$\boldsymbol{Y}_1 \widehat{\boldsymbol{\Theta}}_1 = \widehat{\rho}_c(t) \widehat{V_{r,c}^2} \overline{u}(t) \tag{24}$$

$$\boldsymbol{Y}_2 \widehat{\boldsymbol{\Theta}}_2 = -\widehat{\rho}_t \widehat{V_{r,t}^2} \widehat{C_{b,t}} \tag{25}$$

where $\widehat{\boldsymbol{\Theta}}_1, \widehat{\boldsymbol{\Theta}}_2 \in \mathbb{R}^3$ are the estimates of $\boldsymbol{\Theta}_1$ and $\boldsymbol{\Theta}_2$, $\widehat{\rho_i}(t) = \widehat{D_{1,i}} + \widehat{D_{2,i}} sin(\Omega t) + \widehat{D_{3,i}} cos(\Omega t)$, $\widehat{D_{1,i}}, \widehat{D_{2,i}}, \widehat{D_{3,i}}, \widehat{V_{r,i}^2}$ and $\widehat{C_{b,t}}$ are the estimates of $D_{1,i}, D_{2,i}, D_{3,i}, V_{r,i}^2$ and $C_{b,t}$, with $i = c, t$, respectively.

Based on equations (14), (24) and (25), and the subsequent stability analysis, the controller is designed as

$$\overline{u}(t) = \left(\widehat{\rho_c}(t) \widehat{V_{r,c}^2}\right)^{-1} \left(\widehat{\rho_t}(t) \widehat{V_{r,t}^2} \widehat{C_{b,t}} - \boldsymbol{K_{LQR}} \boldsymbol{X}\right) \tag{26}$$

where $\boldsymbol{K_{LQR}} \in \mathbb{R}^4$ is a vector of constant gains and $\boldsymbol{X} \in \mathbb{R}^4$ is the measurable state vector defined in equation (14). The estimation errors $\widetilde{\boldsymbol{\Theta}}_1$ and $\widetilde{\boldsymbol{\Theta}}_2$ are defined as

$$\widetilde{\boldsymbol{\Theta}}_1 = \boldsymbol{\Theta}_1 - \widehat{\boldsymbol{\Theta}}_1 \tag{27}$$

$$\widetilde{\boldsymbol{\Theta}}_2 = \boldsymbol{\Theta}_2 - \widehat{\boldsymbol{\Theta}}_2 \tag{28}$$

Therefore, equation (17) can be rewritten as

$$u_y = \boldsymbol{Y}_1 \widetilde{\boldsymbol{\Theta}}_1 + \boldsymbol{Y}_1 \widehat{\boldsymbol{\Theta}}_1 + \boldsymbol{Y}_2 \widetilde{\boldsymbol{\Theta}}_2 + \boldsymbol{Y}_2 \widehat{\boldsymbol{\Theta}}_2 \tag{29}$$

The adaptive update laws $\dot{\widehat{\boldsymbol{\Theta}}}_1$ and $\dot{\widehat{\boldsymbol{\Theta}}}_2$ are designed as

$$\dot{\widehat{\boldsymbol{\Theta}}}_1 = \text{proj}\left(2\Gamma_1 Y_1^T B^T P^T X\right) \tag{30}$$

$$\dot{\widehat{\boldsymbol{\Theta}}}_2 = 2\Gamma_2 \boldsymbol{Y}_2^T \boldsymbol{B}^T P^T \boldsymbol{X} \tag{31}$$

the vector $\boldsymbol{B} \in \mathbb{R}^4$ is defined in equation (14), $P \in \mathbb{R}^{4\times4}$ is a symmetric positive definite matrix defined in the subsequent stability analysis, Γ_1, $\Gamma_2 \in \mathbb{R}^{3\times3}$ are the adaptation gains for $\widehat{\boldsymbol{\Theta}}_1$ and $\widehat{\boldsymbol{\Theta}}_2$, respectively. The operator $\text{proj}(\cdot)$ is the continuous projection algorithm developed in Ref. [28] used here to keep $\widehat{\boldsymbol{\Theta}}_1(t)$ within the bounds shown in equation (22), this is especially important to ensure that the inverse of $(\widehat{\rho_c}(t)\widehat{V_{r,c}^2})$, which is present in the control law of equation (26), does not cross zero.

4. Stability analysis

Theorem 1. Given the relative dynamics in equation (14) along with the adaptive update laws in equations (30) and (31), the controller in equation (26) yields local asymptotic regulation in the sense that

$$\lim_{t\to\infty} ||\boldsymbol{X}|| \to 0. \tag{32}$$

Proof. Let $V : \mathbb{R}^{10} \to \mathbb{R}_{\geq 0}$ be a candidate Lyapunov function defined as

$$V(\boldsymbol{\eta}) = \boldsymbol{X}^T P \boldsymbol{X} + \frac{1}{2}\widetilde{\boldsymbol{\Theta}}_1^T \Gamma_1^{-1} \widetilde{\boldsymbol{\Theta}}_1 + \frac{1}{2}\widetilde{\boldsymbol{\Theta}}_2^T \Gamma_2^{-1} \widetilde{\boldsymbol{\Theta}}_2 \tag{33}$$

where the composite state vector $\boldsymbol{\eta} \in \mathbb{R}^{10}$ is

$$\boldsymbol{\eta} = \left[\boldsymbol{X}^T \ , \ \widetilde{\boldsymbol{\Theta}}_1^T \ , \ \widetilde{\boldsymbol{\Theta}}_2^T\right]^T \tag{34}$$

For analysis purposes the auxiliary input u_y can be divided in two terms as follows

$$u_y = u_{FB} + u_{AD} \tag{35}$$

where $u_{FB} \in \mathbb{R}$ is a state feedback term and $u_{AD} \in \mathbb{R}$ is a term used for adaptation purposes.

From the in-plane SS dynamics in equation (14), the rank of the controllability matrix can be computed to observe that the system is controllable with the single input u_y. Motivated by the fact that this is an underactuated system with a single input and four states to be regulated, and by the results obtained in Refs. [9], a Linear Quadratic Regulator (LQR) is designed to obtain a state feedback control law that regulates all states of the SS dynamics to zero while minimizing the cost function

$$J = \int_0^\infty \left(\boldsymbol{X}^T \boldsymbol{Q}\boldsymbol{X} + R u_{FB}^2\right) dt \tag{36}$$

where $Q \in \mathbb{R}^{4\times4}$ is a positive definite weight matrix used to specify the desired performance of each state in $\boldsymbol{X}$ and $R \in \mathbb{R}_{>0}$ is a weight used to penalize the control effort. The state feedback control law is defined as

$$u_{FB} = -\boldsymbol{K_{LQR}}\boldsymbol{X} \tag{37}$$

where $\boldsymbol{K_{LQR}} \in \mathbb{R}^4$ is a constant feedback gain vector obtained from solving the Algebraic Riccati Equation (ARE) [29].

Plugging-in the dynamics from equation (14), the definition of the auxiliary control input u_y from equation (35) and the state feedback control law from equation (37) in the time derivative of equation (33) yields

$$\dot{V}(\boldsymbol{\eta}) = \boldsymbol{X}^T\left(PA^* + A^{*T}P\right)\boldsymbol{X} + 2\boldsymbol{X}^T P\boldsymbol{B}u_{AD} - \widetilde{\boldsymbol{\Theta}}_1^T\Gamma_1^{-1}\dot{\widehat{\boldsymbol{\Theta}}}_1 - \widetilde{\boldsymbol{\Theta}}_2^T\Gamma_2^{-1}\dot{\widehat{\boldsymbol{\Theta}}}_2 \tag{38}$$

where $A^* = A - \boldsymbol{B}\boldsymbol{K_{LQR}}$ and $A \in \mathbb{R}^{4\times4}$ is defined in equation (14). Note that A^* is Hurwitz since $\boldsymbol{K_{LQR}}$ is obtained by solving the LQR problem. Therefore, a symmetric positive definite matrix $Q_1 \in \mathbb{R}^{4\times4}$ can be used so that the Lyapunov equation (39) is satisfied.

$$PA^* + A^{*T}P = -Q_1 \tag{39}$$

Then, $\dot{V}(\boldsymbol{\eta})$ can be rewritten as

$$\dot{V}(\boldsymbol{\eta}) = -\boldsymbol{X}^T Q_1 \boldsymbol{X} + 2\boldsymbol{X}^T P\boldsymbol{B}u_{AD} - \widetilde{\boldsymbol{\Theta}}_1^T\Gamma_1^{-1}\dot{\widehat{\boldsymbol{\Theta}}}_1 - \widetilde{\boldsymbol{\Theta}}_2^T\Gamma_2^{-1}\dot{\widehat{\boldsymbol{\Theta}}}_2 \tag{40}$$

Solving equation (35) for u_{AD} and plugging-in u_y from equation (29) yields

$$u_{AD} = \boldsymbol{Y}_1\widetilde{\boldsymbol{\Theta}}_1 + \widehat{\rho_c}(t)\widehat{V_{r,c}^2}\overline{u}(t) + \boldsymbol{Y}_2\widetilde{\boldsymbol{\Theta}}_2 - \widehat{\rho_t}(t)\widehat{V_{r,t}^2}\widehat{C_{b,t}} + \boldsymbol{K_{LQR}}\boldsymbol{X} \tag{41}$$

Finally, substituting equations (26), (30), (31) and (41) in the Lyapunov derivative we obtain

$$\dot{V}(\boldsymbol{\eta}) = -\boldsymbol{X}^T Q_1 \boldsymbol{X} \tag{42}$$

From equation (42), $\dot{V}$ is negative semi-definite, indicating that $V \in L_\infty$. Therefore, $\boldsymbol{X}, \widetilde{\boldsymbol{\Theta}}_1, \widetilde{\boldsymbol{\Theta}}_2 \in L_\infty$, and then $\boldsymbol{\eta} \in L_\infty$. Using equations (27) and (28), $\widehat{\boldsymbol{\Theta}}_1$, $\widehat{\boldsymbol{\Theta}}_2 \in L_\infty$. Since $\sin(\Omega t), \cos(\Omega t) \in L_\infty$ by definition, then the estimated atmospheric density $\widehat{\rho_c}(t)$, $\widehat{\rho_t}(t) \in L_\infty$. Therefore, the controller in equation (26), $\overline{u} \in L_\infty$. Since $\overline{u} \in L_\infty$, using equation (29), $\boldsymbol{Y}_1 \in L_\infty$ and then $\dot{\boldsymbol{X}} \in L_\infty$. Since $\dot{\boldsymbol{X}} \in L_\infty$, then $\boldsymbol{X}$ is uniformly continuous and from equation (42), $\boldsymbol{X} \in L_2$. Therefore, by Barbalat's Lemma [30].

$$\lim_{t\to\infty} \|\mathbf{X}\| \to 0 \tag{43}$$

Note that this result does not guarantee that the estimated parameters $\widehat{\boldsymbol{\Theta}}_1$ and $\widehat{\boldsymbol{\Theta}}_2$ converge to their true values. In fact, it only ensures that the estimation errors $\widetilde{\boldsymbol{\Theta}}_1$ and $\widetilde{\boldsymbol{\Theta}}_2$ remain bounded during the maneuver. Therefore, the control design presented in this paper is only intended to provide guarantee of states regulation without ensuring on-line parameter estimation.

5. Numerical simulations

To validate the developed control law (equation (26)), the numerical simulations are divided in two cases. The first case evaluates the performance of the control law using the SS dynamics used for the controller design. On the other hand, the second case evaluates the controller performance using the nonlinear dynamics of equations (1)–(3) for each spacecraft as well as some additional sources of uncertainty. In both cases, the initial conditions are selected such that the chaser spacecraft is in a circular orbit similar to that of the International Space Station (ISS) (see Table 1), while the initial conditions of the target are randomly selected by varying the chaser's semi-major axis a_c, eccentricity e_c and true anomaly ν_c so that the inter-spacecraft distance satisfies assumption 1, while the RAAN (Ω_c), argument of perigee (ω_c) and orbit inclination (i_c) remain unchanged for both spacecraft. The bounds for such variations are as follows.

- $a_t = a_c \pm 500$ $[m]$
- $e_t = e_c + 5\times10^{-5}$
- $\nu_t = \nu_c \pm 0.2$ $[deg]$

The gain $\boldsymbol{K_{LQR}}$ has been computed using the *lqr* command in Matlab with the SS dynamics (equation (14)) and the values for the matrices Q and R from Ref. [9] and shown in Table 2. The solution of the ARE is used as value for matrix P and the adaptive gains Γ_1 and Γ_2 are also shown in Table 2. The physical parameters for the chaser spacecraft and for the unknown target used in the numerical simulations are presented in Table 3.

5.1. Results with SS dynamics

The numerical simulations using the SS dynamics are intended to evaluate the controller performance under the same assumptions made during the control design. However, in order to keep the maneuver feasible for a D3-equipped chaser spacecraft, saturation is applied to the control input $\overline{u}$ (ballistic coefficient) so that the cross sectional area S_c is always between $S_{c,min}$ and $S_{c,max}$. Given that the relative states do not provide enough information to feed an atmospheric density model, values for the parameters $D_{1,i}, D_{2,i}$ and $D_{3,i}$ (shown in Table 4) were found offline by fitting the model of equation (13) to density data obtained from the NRLMSISE-00 atmospheric model when propagating the chaser spacecraft with the drag surfaces deployed halfway. Although this is only an approximation, it is important to mention that the density is only used to propagate the relative dynamics and not to compute the control law.

The resulting relative states from the numerical simulation are shown in Fig. 3. The plots in the left show the behavior of relative states over time while the one in the right shows the relative path in the LVLH coordinate system. From these results, it can be observed that the relative states converge to zero and the total maneuver time was 60 h. Fig. 4 shows the control command (chaser's ballistic coefficient) as well as the unknown ballistic coefficient of the target over time. The control command plot shows that the controller is able to adapt so that at the end of the maneuver the differential drag is zero.

The behavior of the estimated parameters $\widehat{\boldsymbol{\Theta}}_1$ and $\widehat{\boldsymbol{\Theta}}_2$ is shown in Fig. 5. Although the stability analysis does not ensure that the estimated parameters converge to the real values, they remain bounded and converge to some values that enable the controller to drive the system to the origin.

5.2. Results with complete dynamics

The simulations with the spacecraft complete dynamics propagates equations (1)–(3) individually for each spacecraft. The atmospheric density is now locally computed for each spacecraft using the NRLMSISE-00 model and the rotation of the atmosphere with the Earth is also taken into account to compute the vector $\boldsymbol{V_r}$ for each spacecraft. Additionally, a 5 $[RPM]$ sinusoidal perturbation of 10% the magnitude of $C_{b,t}$ is introduced to simulate a tumbling target. At each time step during the propagation the relative states are computed so that the control and update laws can be computed.

Fig. 6 shows the resulting relative states from the simulation. From this figure, it is observed that the adaptive controller is able to regulate the relative relative states even using the complete dynamics and the total maneuver time in this case was 62 h. Fig. 7 shows the control command (ballistic coefficient of the chaser) as well as the ballistic coefficient of the target. From the control command plot, the ballistic coefficient of the chaser ($C_{b,c}$) converges to the mean value of $C_{b,t}$ so that

the differential drag at the end of the maneuver is as close as possible to zero considering that $C_{b,t}$ was modeled as a constant parameter in the controller design.

Finally, the behavior of the estimated parameters $\widehat{\boldsymbol{\Theta}}_1$ and $\widehat{\boldsymbol{\Theta}}_2$ over time is shown in Fig. 8. As in the case with the SS dynamics, the estimated parameters remain bounded and converge to some values that are not necessarily the real ones. It is also important to note that in this case there are no real values for the parameters $D_{1,i}, D_{2,i}$, $D_{3,i}$, or constant values for $V_{r,i}$ or $C_{b,t}$ because these were approximations made in the controller design. However, these assumptions have shown to be sufficient for the purpose of regulating the in-plane relative dynamics.

6. Conclusion

A novel Lyapunov-based adaptive controller has been designed to address the problem of performing differential drag-based rendezvous with a non-cooperative target in LEO. The control design includes adaptive update laws to ensure regulation of the relative states in presence of uncertain time-varying atmospheric density, target ballistic coefficient and magnitude of the spacecraft's velocity with respect to the atmosphere. Numerical simulations were performed using the Schweighart-Sedwick equations of relative motion as well as using a more complete dynamic model which does not include assumptions made during the controller design. The results in both cases have shown that the adaptive control law successfully regulates the in-plane relative states even under input saturation. Future efforts will include exploring the use of new adaptive update laws that guarantee some level of on-line parameter estimation.

Acknowledgments

This research has been supported by the Fulbright Colombia Commission and the AFOSR award number FA9550-19-1-0169. Any opinions, findings and conclusions or recommendations expressed in this material are those of the authors and do not necessarily reflect the views of the sponsoring agency.

References

[1] NASA, Process for limiting orbital debris, in: Tech. Rep. nasa-std-8719.14a, 2012, 2012.
[2] C.L. Leonard, W.M. Hollister, E.V. Bergman, Orbital formationkeeping with differential drag, J. Guid. Contr. Dynam. 12 (1) (1989) 108–113, https://doi.org/10.2514/3.20374.
[3] R. Bevilacqua, M. Romano, Rendezvous maneuvers of multiple spacecraft by differential drag under J2 perturbation, J. Guid. Contr. Dynam. 31 (6) (2008) 1595–1607, https://doi.org/10.2514/1.36362.
[4] M. Horlsey, S. Nikolaev, A. Pertica, Rendezvous maneuvers of small spacecraft using differential lift and drag, J. Guid. Contr. Dynam. 36 (2) (2011) 445–453, https://doi.org/10.2514/1.57327.
[5] M.W. Harris, B. Akmee, Minimum time rendezvous of multiple spacecraft using differential drag, J. Guid. Contr. Dynam. 37 (2) (2014) 365–373, https://doi.org/10.2514/1.61505.
[6] D. Perez, R. Bevilacqua, Differential drag spacecraft rendezvous using an adaptive Lyapunov control strategy, Acta Astronaut. 83 (2012) 196–207, https://doi.org/10.1016/j.actaastro.2012.09.005.
[7] D. Ivanov, M. Kushniruk, M. Ovchinnikov, Study of satellite formation flying control using differential lift and drag, Acta Astronaut. 152 (2018) 88–100, https://doi.org/10.1016/j.actaastro.2018.07.047.
[8] S. Varma, K.D. Kumar, Multiple satellite formation flying using differential aerodynamic drag, J. Spacecraft Rockets 49 (2) (2012) 325–336, https://doi.org/10.2514/1.52395.
[9] C. Riano-Rios, R. Bevilacqua, W.E. Dixon, Relative maneuvering for multiple spacecraft via differential drag using lqr and constrained least squares, in: AAS/AIAA Space Mechanics Meeting, Ka'anapali, HI, 2019.
[10] T.D. Maclay, C. Tuttle, Satellite stationkeepong of the ORBCOMM constellation via active control of atmospheric drag: operations, constraints and performance, Adv. Astronaut. Sci. 120 (1) (2005) 763–774.
[11] C. Foster, J. Mason, V. Vittaldev, V. Beukelaers, L. Stepan, R. Zimmetman, Constellation phasing with differential drag on Planet Labs satellites, J. Spacecraft Rockets 55 (2) (2018) 473–483, https://doi.org/10.2514/1.A33927.
[12] S. D'Amico, J.S. Ardaens, G. Gaias, H. Benninghoff, B. Schlepp, J.L. Jrgensen, Noncooperative rendezvous using angles-only optical navigation: system design and flight results, J. Guid. Contr. Dynam. 36 (6) (2013) 1576–1595, https://doi.org/10.2514/1.59236.
[13] J. Telaar, C. Schlaile, J. Sommer, Guidance and navigation for rendezvous with an uncooperative target, Progress in Flight Dynamics, Guidance, Navigation, and Control 10 (2018) 3–20, https://doi.org/10.1051/eucass/201810003.
[14] M. Richard, L.G. Kronig, F. Belloni, V. Gass, O.A. Araromi, I. Gavrilovich, H. Shea, C. Paccolat, J.-P. Thiran, Uncooperative rendezvous and docking for microsats, in: 6th International Conference on Recent Advances in Space Technologies, RAST, Istambul, Turkey, 2013, 2013.
[15] D. Zhang, S. Song, R. Pei, Safe guidance for autonomous rendezvous and docking with a non-cooperative target, in: AIAA Guidance, Navigation, and Control Conference, Toronto, Ontario, Canada, 2010.
[16] G. Gaias, J.-S. Ardaens, Flight demonstration of autonomous noncooperative rendezvous in low earth orbit, J. Guid. Contr. Dynam. 41 (6) (2017) 1337–1354, https://doi.org/10.2514/1.G003239.
[17] S.F. Rafano, S. Omar, D. Guglielmo, R. Bevilacqua, Safety analysis for shallow controlled spacecraft Re-entry using aerodynamic drag, Acta Atronautica 155 (2018) 426–447, https://doi.org/10.1016/j.actaastro.2018.10.015.
[18] S. Omar, D. Guglielmo, R. Bevilacqua, Drag de-orbit device (d3) mission for validation of controlled spacecraft re-entry using aerodynamic drag, in: 4th IAA Dynamics and Control of Space Systems Conference, Rome, Italy, 2017.
[19] S. Omar, D. Guglielmo, G. Di Mauro, T. Martin, R. Bevilacqua, Cubesat mission to demosntrate aerodynamically controlled re-entry using the drag de-orbit device (d3), in: SmallSat Conference 2018, Logan, UT, 2018.
[20] S. Omar, C. Riano-Rios, R. Bevilacqua, Semi-passive three axis attitude stabilization for earth observation satellites using the drag maneuvering device, in: 12th Symposium on Small Satellite for Earth Observation. Berlin, Germany. 2019, 2019.
[21] C. Riano-Rios, S. Omar, R. Bevilacqua, W. Dixon, Spacecraft attitude regulation in low earth orbit using natural torques, in: 2019 IEEE 4th Colombian Conference on Automatic Control (CCAC), Medellin, Colombia, 2019.
[22] S.A. Schweighart, R.J. Sedwick, High-fidelity linearized J2 model for satellite formation flight, J. Guid. Contr. Dynam. 25 (6) (2002) 1073–1080, https://doi.org/10.2514/2.4986.
[23] U.s NOAA, Standard Atmosphere, 1976 (1976).
[24] I. Harris, W. Priester, Time-dependent structure of the upper atmosphere, J. Atmos. Sci. 19 (4) (1962) 286–301, https://doi.org/10.1175/1520-0469(1962)019<0286:TDSOTU>2.0.CO;2.
[25] J.M. Picone, A.E. Hedin, D.P. Drob, A.C. Aikin, NRLMSISE-00 emprical model of the atmosphere: statistical comparisons and scientific issues, J. Geophys. Res. 107 (A12) (2002), https://doi.org/10.1029/2002JA009430, 15–1–15–16.
[26] O. Montenbruck, E. Gill, Satellite Orbits: Models, Methods and Applications, Springer, Berlin, 2000.
[27] G. Gaias, J.-S. Ardaens, O. Montenbruck, Model of J2 perturbed satellite relative motion with time-varying differential drag, Celestial Mech. Dyn. Astron. 123 (2015), https://doi.org/10.1007/s10569-015-9643-2, 441–433.
[28] W.E. Dixon, A. Behal, D.M. Dawson, S. Nagarkatti, Nonlinear Control of Engineering Systems: A Lyapunov-Based Approach, Birkhauser, Boston, 2003.
[29] J.P. Hespanha, Linear Systems Theory, second ed., Princeton University Press, 2018.
[30] H.K. Khalil, Nonlinear Systems, third ed., Prentice Hall, NJ, 2002.